Spectral Analysis of Gappy Images With Application to SeaWiFS Data

July 18, 2000

Roman E. Glazman, Jet Propulsion Laboratory 300-323G, California Institute of Technology, Pasadena, CA 91125

To be presented at IGARSS 2000, Honolulu, HI. July 23-29.

1 Introduction

For various reasons, such as the presence of clouds (for visible and IR bands), satellite orbit configuration, data sampling pattern, missing or bad measurements, etc., remote sensing instruments yield irregularly spaced (in time and over an ocean area) or gappy/patchy measurements. Usually, these measurements are interpolated onto a regular (spatial and temporal) grid or accumulated over some time intervals to yield composite images such as weekly, monthly, or yearly geographic distributions of an oceanographic quantity. However, for some studies - especially for spectral analysis of oceanographic fields - neither interpolation nor "composition" produce satisfactory input data because both techniques reduce spatial and temporal resolution and distort patterns of spatial and temporal variability of an oceanographic field. To obviate these problems, we use original, non-gridded satellite data, as described for the case of altimeter measurements in [Glazman et al., (1996) in Int. J. Rem. Sens., 17, 2647-66], and construct a spatio-temporal (or just spatial) autocorrelation function of the field's variation. The spatial and temporal lags for all possible pairs of points are binned onto a regular grid of lags, and the products for each pair are eventually averaged within the bins. The resulting function is fourier- transformed to produce a wavenumber/frequency spectrum. This approach is presently applied to SeaWiFS data to obtain the 2D wavenumber spectrum of Chlorophyll-a variations for various ocean regions. Both the approach and the results are discussed in this talk.

2 Estimaiton of chlorophyll spectra based on SeaWiFS images, and of BIG wave and QG components of the SSH spectrum based on Topex altimeter data

Ocean tracer distributions, such as sea surface temperature or chlorophyll-a concentration fields, are measured from space by passive infrared and visible-light imaging sensors. We shall use the data on chlorophyll concentration from the SeaWiFS instrument (the full name is Sea-viewing Wide Field-of-view Sensor) launched in 1997. These measurements are available with an up

to 1.3 km spatial resolution. Since atmospheric clouds are always present over any sufficiently large ocean area, satellite images have gaps. One such image is illustrated in Fig.B1 where black areas are clouds or otherwise missing data. This ocean region is located about 500 km south of the southern tip of Africa where the strong Agulhas current and its retroflection create a highly intense eddy field.

In order to estimate the power spectrum of Chl-a fluctuations, we first subtract the mean value of Chl-a concentration from local values at each point and then compute products $q(\mathbf{x})q(\mathbf{x}')$ of the differences for all pairs of points $\mathbf{x}$ and $\mathbf{x}'$. These products are binned by narrow intervals (4x4 km^2) of the spatial lag $\mathbf{x} - \mathbf{x}'$ and eventually averaged within each bin to yield an estimate of the spatial autocorrelation function $R(\mathbf{x} - \mathbf{x}')$ (??). For the field in Fig.B1, this function is shown in Fig.B2. The power spectrum is obtained as the 2D fourier transform of $R(\mathbf{x} - \mathbf{x}')$, and employing the Hanning window in order to reduce adverse effects of the finite size of the geographic area and the Chl-a field's spatial inhomogeneity on largest scales. The 2D power spectrum corresponding to Fig.B2 is illustrated in Fig. 5.
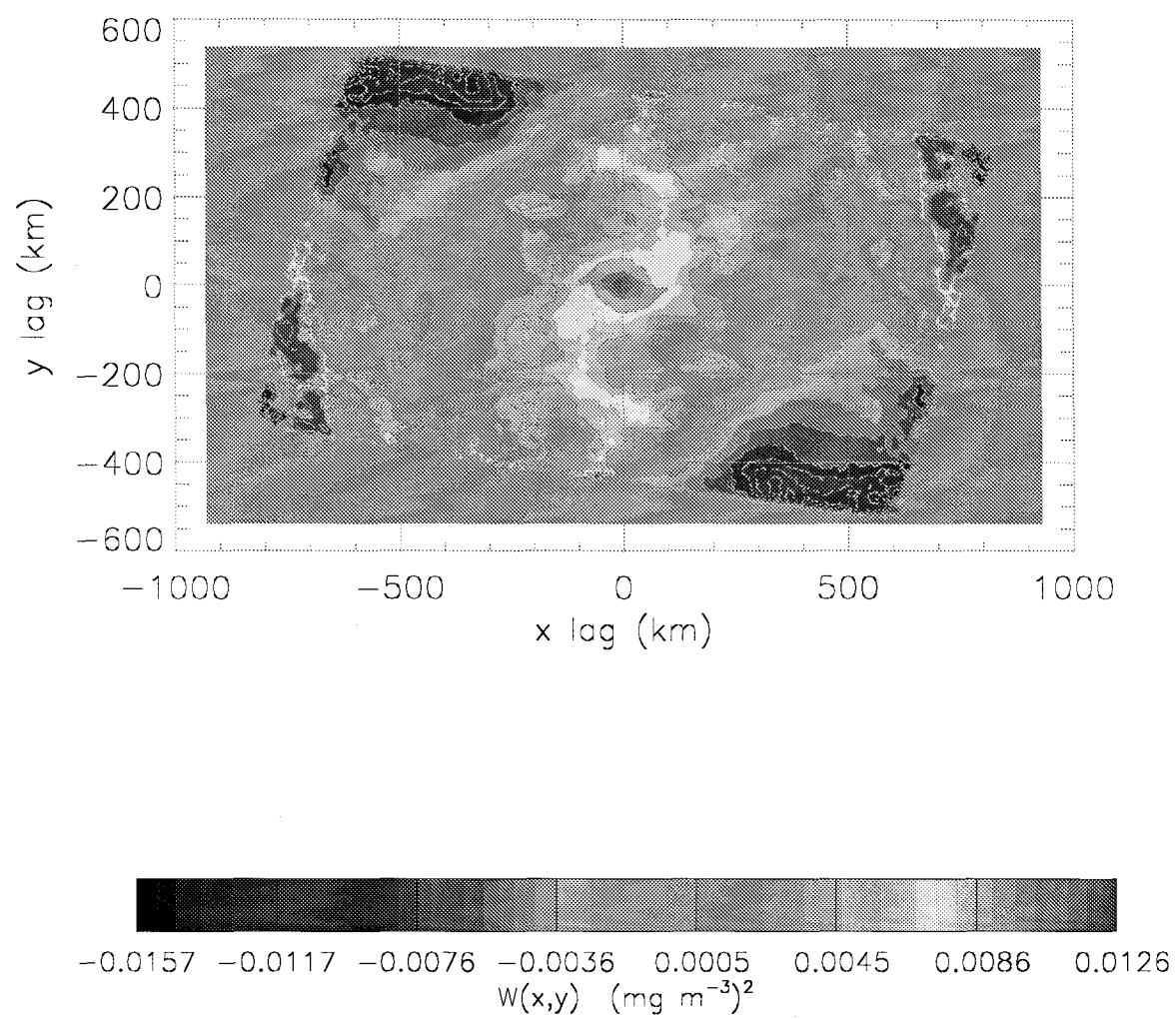
A detailed description of our altimeter data analysis technique is presented in [?] and [?]. Let us explain its key feature - the separation of the observed SSH spectrum into two components representing the slow, quasi-geostrophic, and the fast, inertia-gravity wave, motions. The (Topex) satellite altimeter takes SSH measurements every 6.4 km along its one-dimensional groundtracks on both descending and ascending passes over an ocean area. Within any 10-day interval (the orbit repeat cycle), it covers the world ocean with the grid of groundtrack passes, yielding SSH values $\zeta(\mathbf{x}, t)$ at points $\mathbf{x}$ along the ground tracks. Within a limited surface area, say 10x10 degree squared, we thus obtain a set of $\zeta(\mathbf{x}, t)$ with time differences from 0 (for measurements taken on individual grountrack passes) to 10 days (for measurements taken on different passes within a repeat cycle). Accumulating all such measurements over a sufficiently long (on the timescale of QG motions) time interval - for example, half a year - we then estimate the spatio-temporal autocorrelation function of SSH variations, $W(\mathbf{r}, \tau)$, where $\mathbf{r}$ and τ are the 2D spatial and 1D time lags. In view of the fact that the contribution to this function of the fast, BIG wave component vanishes for τ greater than the charateristic autocorrelation time of BIG wave oscillations, t^*_{BIG} (a few dominant BIG wave periods), we assume $W(\mathbf{r}; \tau \geq t^*_{BIG})$ to be determined solely by the QG motions. Because the characteristic timescale of variations of the 2D vortical velocity field is much greater than t^*_{BIG}, function $W(\mathbf{r}, \tau = t^*_{BIG})$ represents a purely spatial autocorrelation function of the QG component. Its spatial fourier transform yields the wavenumber spectrum of QG motions. We now turn our attention to altimeter measurements on individual passes. For all practical purposes, these measurements can be viewed as instantaneous because the satellite covers a 3000 km ground distance in 3 min. Therefore, 1D spectra of SSH variations along these passes contain contributions of both the fast and the slow components of SSH variability. If we now reduce the 2D spectrum obtained earlier to the 1D form and subtract it from the 1D spectrum of the alongtrack SSH variations, the difference will give us an estimate of the spectrum of the fast motions. It is this spectrum that we plot as a solid curve in Fig. 3, ~~and~~.
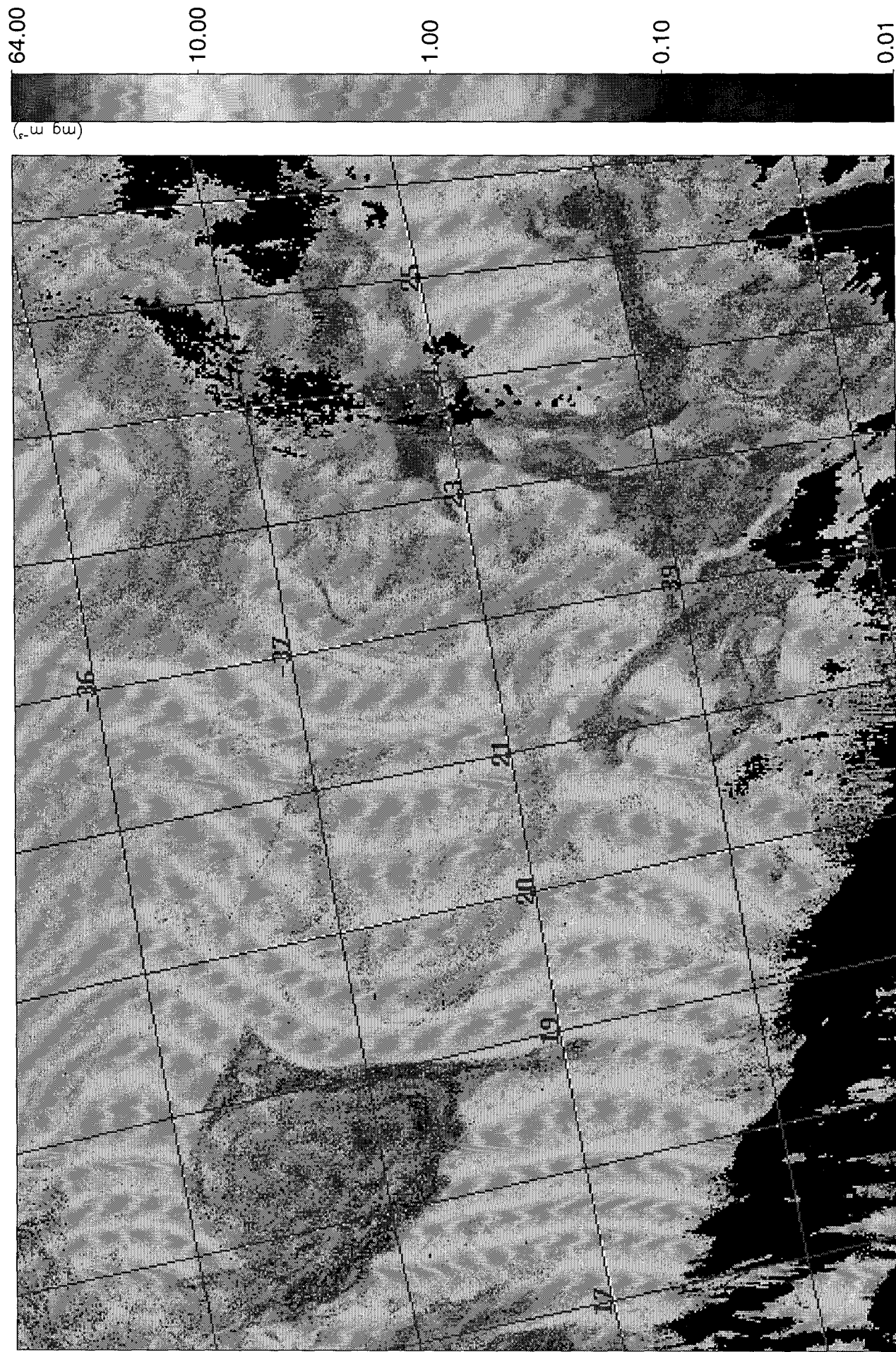
References

[1] Charney, J.G., 1971, *Geostrophic turbulence*, J. Atmos. Sci., **28**(6), 1087.

[2] Denman, K.L. and M.R. Abbott, 1994, *Time scales of pattern evolution from cross-spectral analysis of advanced very high resolution radiometer and coastal zone color scanner imagery*, J. Geophys. Res., **99** (C4), 7433.

[3] Deschamps, P.Y., R. Frouin, and L. Wald, 1981, *Satellite determination of the mesoscale variability of the sea surface temperature*. J. Phys. Oceanogr., **11**, 864.

[4] Fasham, M. J., 1978, *The statistical and mathematical analysis of plankton patchiness*, Oceanogr. Mar. Biol. A. Rev., **16**, 43.

[5] Glazman, R. E., 1996, *Spectra of baroclinic inertia-gravity wave turbulence*, J. Phys. Oceanogr. **26**, 1256.

[6] Glazman, R.E. and B. Cheng, 1998, *Altimeter observations of baroclinic oceanic inertia-gravity wave turbulence*, Proc. Roy. Soc. Lond. Ser. A. (in press).

[7] Herterich, K. and K. Hasselmann, 1982, *The horizontal diffusion of tracers by surface waves*, J. Phys. Oceanogr. **12**(7), 704.

[8] Klyatskin, V.I., 1994. *Statistical description of diffusing tracers in random velocity fields*, Physics-Uspekhi bf 37(5), 501.

[9] Kraichnan, R.H., 1974. *Convection of a passive scalar by a quasi-uniform random straining field*. J. Fluid Mech., **64**(4), 737.

[10] Lesieur M. and R. Sadourny, 1981, *Satellite-sensed turbulent ocean structure*, Nature **294**, 673.

[11] Mirabel, A. P. and S. A. Monin, 1982, *Physics of Oceans and Atmosphere* **19**, 902.

[12] Monin A. S. and A. M. Yaglom, 1971. *Statistical Fluid Mechanics*, Vol.1, 769 pp. MIT Press,

[13] Piterbarg, L. I., 1997, *Short-correlation approximation in models of turbulent diffusion* in: "Stochastic Models in Geosystems" (Springer, New York), S. A. Molchanov and W. A. Wojczinski, editors), p. 313.

[14] Weichman, P. B. and Glazman, R. E., 1998, Passive scalar transport by travelling wave fields (preprint).

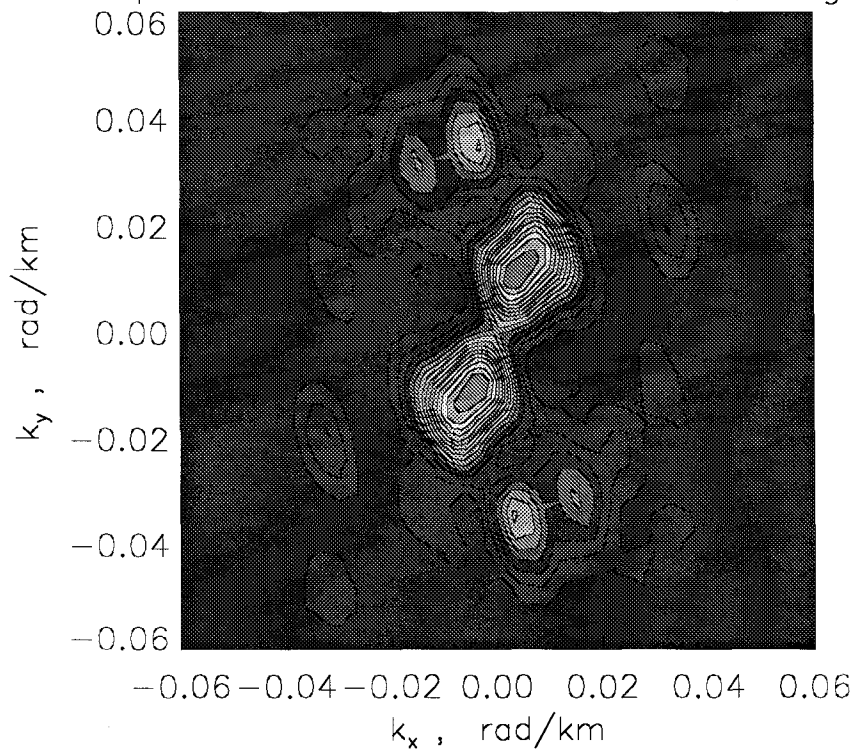[15] I. S. Gradshteyn and I. M. Rhyzhik, *Table of Integrals, Series, and Products* (Academic Press, New York, 1981).

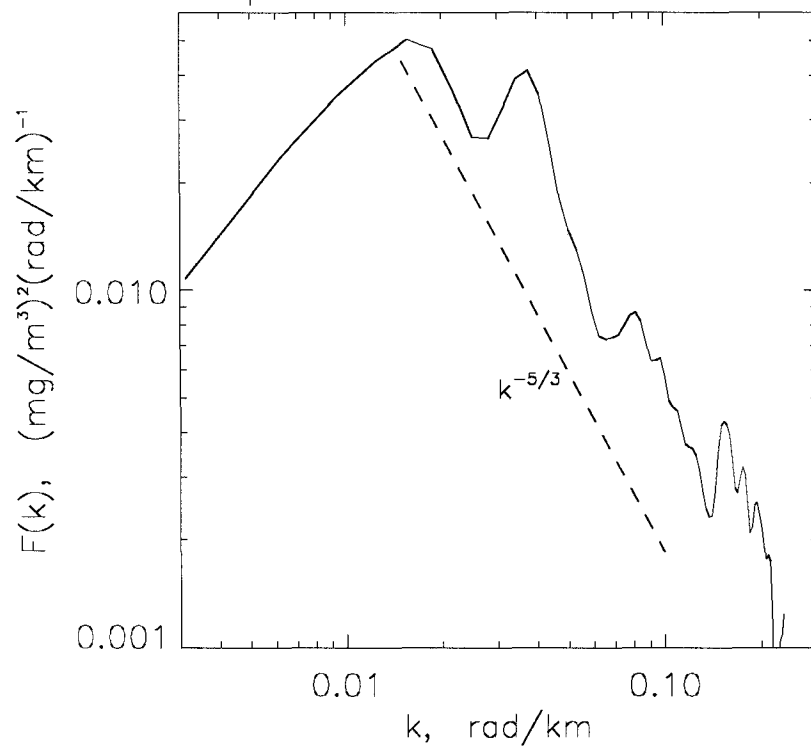## 2D Spatial Autocorrelation Function, W(x,y), for HPRE_8_189

-0.0157 -0.0117 -0.0076 -0.0036   0.0005   0.0045   0.0086   0.0126

$W(x,y)$ $(mg\ m^{-3})^2$

B2

chlor_a : HPRE8_213_A.HDF

(mg m⁻³)

64.00

10.00

1.00

0.10

0.01

2D spectrum of Chl−a variations, Region_A

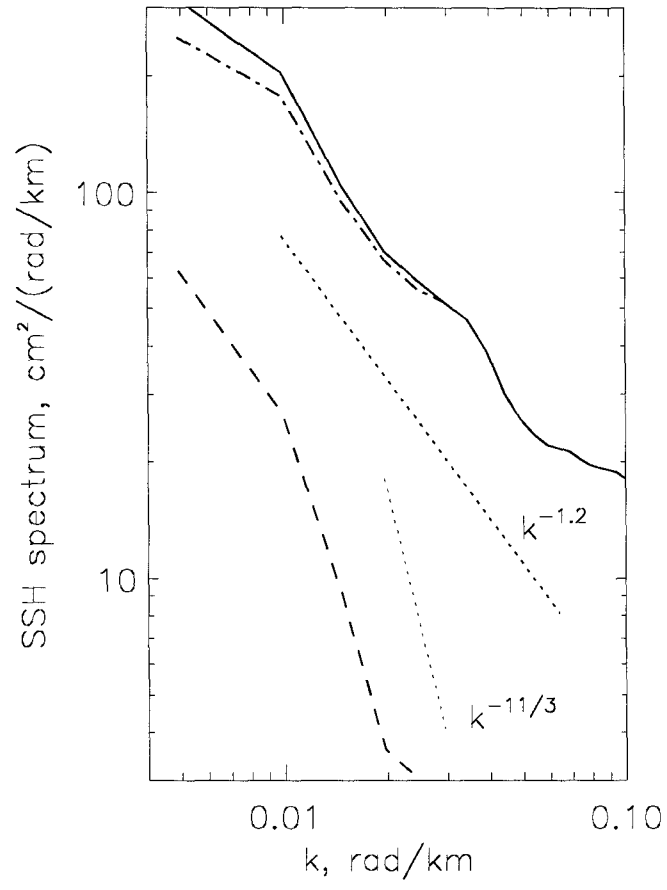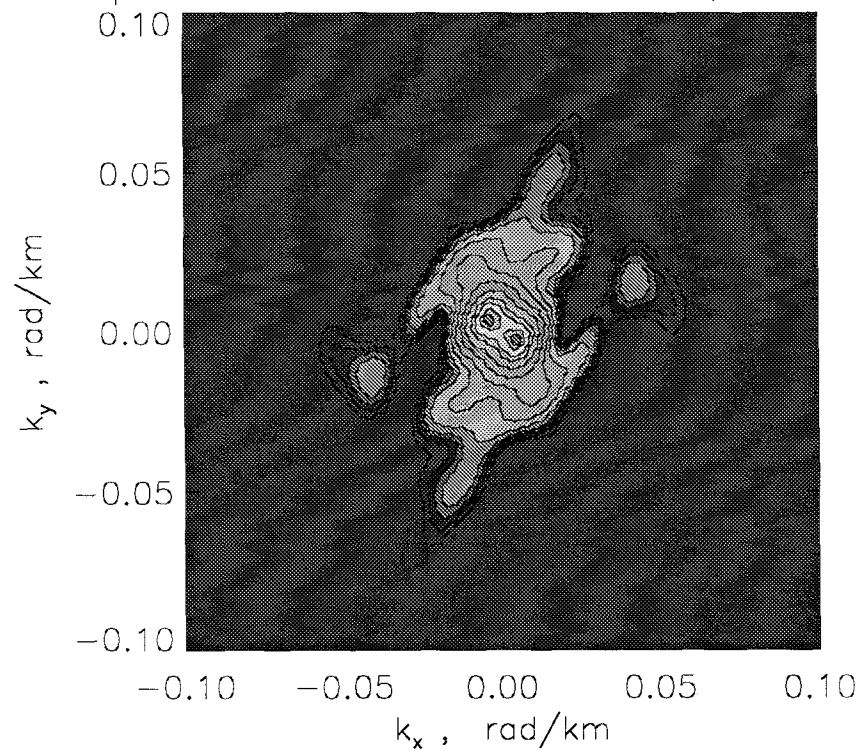## 1D spectrum of Chl−a variations

Fig. 3

2D spectrum of Chl–a variations, HPRE8_189

1D spectrum of Chl–a variations